JOURNAL OF MATERIALS SCIENCE 22 (1987) 3304–3308

Influence of microcracking and homogeneity on the mechanical behaviour of (Al_2O_3 + ZrO_2) ceramics

A. KRELL, P. BLANK, T. WEISS
Academy of Sciences of the German Democratic Republic, Zentralinstitut für Festkörperphysik und Werkstofforschung, Dresden 8027, GDR

Quantitative methods for estimations of microcrack density and dispersion homogeneity give evidence of microcrack generation on macrofracture as the dominating mechanism responsible for toughening. The efficiency of energy dissipation at one microcrack density is higher in zirconia-toughened alumina than in pure Al_2O_3 ceramics. Deterioration of dispersion homogeneity results in the promotion of subcritical crack growth and low strength due to large flaw sizes at instability.

1. Introduction

The toughening effect of the tetragonal–monoclinic phase transformation of ZrO_2 particles dispersed in an alumina matrix has been known for about ten years [1]. Larger tetragonal grains transform spontaneously on cooling of the sintered structure, expand and give rise to the generation of residual stresses which might be useful for an increase in fracture toughness [2]. In fact, however, it is difficult to develop grain-boundary microstructures that are sufficiently strong, and most of the residual stresses relax by delayed microfracture [3]. It is, therefore, more convenient to use a fine-grained dispersion of ZrO_2 because of the higher tetragonal stability of small particles [4]. On macroscopic loading, stress-induced transformation can improve the critical stress intensity (fracture toughness) K_{Ic} alternatively by microcracking (residual stress-induced generation of surfaces) or due to the energy consumption associated with the transformation itself [2, 5]. The present study is intended to give evidence on which of the two mechanisms is dominant in zirconia-toughened alumina (ZTA). Therefore, special attention has been devoted to demonstrating correlations between microcrack density and K_{Ic}.

From the first results published it became clear that structures with poor homogeneity of the dispersed phase commonly exhibit low strength in spite of high toughness [1, 6]. We suppose this behaviour to be due to the subcritical growth of large flaws on loading, promoted by heterogeneously distributed residual stresses: in ZTA the monoclinic ZrO_2 is under hydrostatic compression and, therefore, the main character of residual stress within the alumina matrix is always tension. These tension components cannot be eliminated by any means but will be minimized at ideal homogeneity. It is one of the objectives of this paper to describe quantitatively the influence of dispersion homogeneity on the mechanical behaviour.

2. Experimental procedure

2.1. Materials

Starting with a 0.6 μm Al_2O_3 powder (Alcoa A16SG), granules were prepared by two different technological routes:

(A) After adding milled ZrO_2 powder with agglomerate sizes of 1.1 and 0.65 μm, respectively, the mixture was remilled in a planetary mill (99% Al_2O_3) for one hour, dried and granulated by passing through a 0.63 mm sieve.

(B) ZrO_2 was added to Al_2O_3 as a solution of $ZrOCl_2 \cdot 8H_2O$ in water. The mixture was homogenized in the same mill as above for 4 to 10 h and freeze-dried. Calcination conditions were 950° C for 2 h.

All specimens contained 1400 wt p.p.m. MgO (added as a solution of $MgCl_2 \cdot 6H_2O$) and about 2% of an organic binder. Bars of dimension 5 mm × 8 mm × 60 mm were formed by uniaxial pressing. Most of the samples were sintered at 1560 to 1625° C for 1 h in hydrogen, where for B-route structures the lower temperatures turned out to be more effective in restricting the grain growth of ZrO_2 particles and in improving the strength. Some of the A-route specimens were sintered in air at 1600° C for 2.5 h for comparison.

2.2. Methods

The strength of as-sintered samples and the fracture toughness were measured in three-point bending with 30 mm span length. Notches of 0.21 mm width were fabricated with a high-speed diamond wheel. To heal possibly grinding-induced residual stresses [7], all notched specimens were annealed in air at 1350° C for one hour. Comparing K_{Ic} measured with annealed and unannealed specimens, we found some annealing-induced increase of K_{Ic} for A-route structures associated with an increase of the monoclinic ZrO_2 phase

*This is the average spacing of dispersed monosized, spherical particles.

0022–2461/87 $03.00 + .12 © *1987 Chapman and Hall Ltd.*

TABLE I Effect of notch radius r on measured K_{Ic} of Al_2O_3 ($\bar{D}_L = 2.7\,\mu m$) and B-route ZTA ($\bar{D}_{L,Al_2O_3} \approx 2\,\mu m$, $\bar{D}_{L,ZrO_2} \approx 1\,\mu m$). The specimens had been notched prior to (1) or after (2) sintering. There was no influence of annealing of notched samples for the chosen structures

Material	K_{Ic} (MPa m$^{1/2}$)		
	$r = 55\,\mu m$ (1)	$r = 75\,\mu m$ (1)	$r = 105\,\mu m$ (2)
Al_2O_3	3.85 ± 0.15	4.36 ± 0.10	4.89 ± 0.18
Al_2O_3 + 11.5 vol % ZrO_2	5.82 ± 0.19	–	7.15 ± 0.42
Al_2O_3 + 15.0 vol % ZrO_2	4.98 ± 0.25	–	5.74 ± 0.16

contents X_m (X-ray analysis with Cu$K\alpha$). On the other hand, for B-structures annealing was almost without any effect on either K_{Ic} and X_m. In spite of these problems, compared to identation strength-in-bending (ISB) we prefer the notched beam technique (NBT): ISB gives valuable results for ceramics with stable phases, but with a metastable ZrO_2 component the essential conditions of residual stress-free surfaces [8, 9] and constant subsurface deformation volume at given indenter load [10] are not met. Hence, we tried to introduce narrow notches without changing the ZrO_2 phase characteristic by notching the green (unsintered) compacts with a razor blade. After sintering the notch radius was $r \approx 50$ to $55\,\mu m$. No exaggerated grain growth was observed below the notch tip of fractured specimens. Structures without annealing-induced changes in phase contents and K_{Ic} (Al_2O_3, B-route ZTA) indicated the same toughness at one notch radius $r \approx 100\,\mu m$ independently of whether they had been notched in the green or in the sintered state. Thus, a possible special effect of notching prior to sintering can be excluded.

Comparing results for different structures which all had a strength of 400 to 450 MPa when tested in the as-sintered state, Table I reveals almost the same K_{Ic} (Al_2O_3 + ZrO_2)/K_{Ic} (Al_2O_3) at $r = 55$ and $105\,\mu m$. The average grain size of the Al_2O_3 examined is $\bar{D}_L = 2.7\,\mu m$ as given by the intercept technique on as-sintered surfaces; for this material the dependence of K_{Ic} on notch radius can be well described by $K_{Ic} = [1.12 + 3.7(r/r_0)^{1/2}]$ MPa m$^{1/2}$ with $r_0 = 100\,\mu m$. Therefore, we conclude that the K_{Ic} values reported in the following ($r = 105\,\mu m$, conventionally notched and annealed specimens) describe well the relations between structures, but should be reduced to "true" values approximately according to the results of Table I.

The densities of arbitrarily oriented microcracks in the centre of the transformation zone passing through the structure with the macrocrack tip were measured on replica micrographs taken from macroscopic fracture surfaces. On such micrographs cracks can be distinguished from uncracked grain boundaries by dark artefacts of the foil [11]. The absolute and relative microcrack densities are given by

$$\varrho_{mc} = N_{mc} \langle l \rangle^3 \cong \sum_i l_i^2/A \quad (1)$$

$$\varrho_{mc}^{rel} = 0.742\, N_{Lmc}/N_{Lgb} \quad (2)$$

where N_{mc} and $\langle l \rangle$ are the specific frequency and average length of microcracks, respectively, l_i are the individual crack lengths as seen on the analysed area A (interconnected crack systems have been treated as one large crack), and N_{Lmc}, N_{Lgb} are respectively the number of cracks and grain boundaries (with and without cracks) along some given line. Details of the procedure and comparisons with more complicated methods of analysis are given elsewhere [12]. For Al_2O_3 rational correlations between ϱ_{mc} and the mechanical behaviour have been reported previously [13, 14].

Young's modulus E we derived from the resonance frequency of sintered bars. Assuming as characteristic values of dense, crack-free structures $E_{0,Al_2O_3} = 400$ GPa and $E_{0,ZrO_2} = 230$ GPa, the density of spontaneously generated, randomly oriented penny-shaped microcracks can be estimated [15] from

$$E/E_0 = 1 - \tfrac{2}{9}\varrho_{abs}^{sp} \quad (3)$$

where for E_0 the actual content of ZrO_2 has to be taken into account.

The homogeneity H_{rel} of the relative mutual arrangement of ZrO_2 particles was determined by dividing the analysed area into n squares of length* $a = \frac{2}{3}\bar{D}_{L,ZrO_2}(1 - V)/V$ and counting the number x_i of particles within each (V = volume content of ZrO_2). The standard deviation s of this x_i distribution characterizes the homogeneity if it is related to the average $\bar{x}$. Thus, the relative homogeneity is the reciprocal coefficient of variation

$$H_{rel} = \bar{x}/s \quad (4)$$

With some given value for H_{rel} and a constant volume content V, that structure with the smallest grain size $\bar{D}_{L,ZrO_2}$ of the dispersed phase will exhibit the highest homogeneity of the absolute spatial distribution. Therefore, we need a second parameter of homogeneity

$$H_{abs} = 1/\bar{D}_{L,ZrO_2} \quad (5)$$

Further comments on Equations 4 and 5 are given elsewhere [16]. It is essential to note that H_{abs} is introduced as a pure parameter of homogeneity which is not intended to describe the effect of the grain-size-dependent ZrO_2 phase transformation.

2. Experimental results

Fig. 1 correlates for A-route structures the measured microcrack densities with the associated critical stress intensities K_{Ic}. Absolute and relative representations of the microcrack densities show the same trends; the accuracy of individual measurements (given in Fig. 1 at 11.5 vol % ZrO_2) is quite high. In spite of this good reliability the results do not correlate with K_{Ic} at higher volume contents. The obvious reason is the documented growing degree of spontaneous microcracking which, starting at $V = 11.5$ vol %, causes increasing relaxation of residual stresses at diminishing

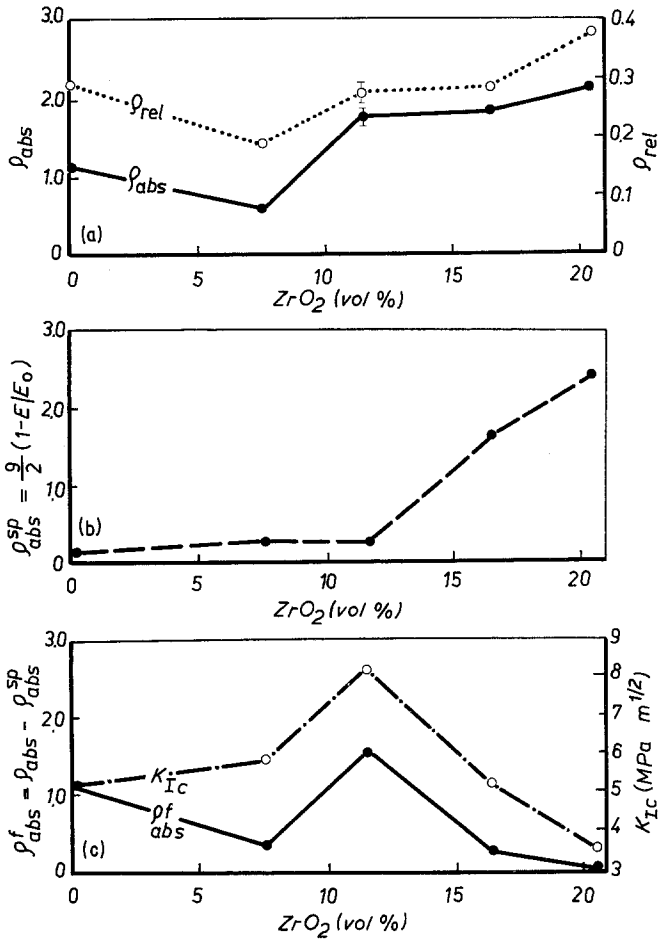

Figure 1 (a) Absolute and relative microcrack densities measured on fracture surfaces, (b) density of spontaneous microcracking, and (c) absolute microcrack density ϱ^{f}_{abs} generated on macrofracture, as compared with fracture toughness K_{Ic}. At optimum K_{Ic} (11.5 vol % ZrO_2) the tetragonal contents is $X_t = 0.49$ in the as-sintered state and $X_t = 0.31$ after annealing at 1350° C for 1 h in air.

tetragonal (transformable on fracture) ZrO_2 contents. Subtraction of the spontaneously formed microcracks gives the density of cracking effective on macrofracture, and this final curve agrees quite favourably with the toughness data. For pure Al_2O_3 we used previous data [13] representing a structure with energy dissipation due to an optimized bidisperse grain size distribution, which explains the somewhat high crack density at 0 vol % ZrO_2 in comparison with 7.5 vol %.

Since fracture strength was measured on as-sintered specimens, most estimations of homogeneity were performed on such surfaces. Figs 2 and 3 demonstrate the improvement of homogeneity if successively finer ZrO_2 particles are introduced (all samples sintered in H_2). The quantitative analysis reveals highest H_{rel} and H_{abs} for the B-route structures with best mechanical properties, but there is no general correlation valid for all examples [16]. Fairly good correspondence, however, results if H_{rel} and H_{abs} are combined empirically as given in Fig. 4. Following the well-known principles of fracture mechanics we used $(K_{Ic}/\sigma_f)^2$ to describe the size of the worst flaw at its instability point. Since the original flaw sizes of all the structures should be similar due to the same forming technology applied for all specimens, Fig. 4 demonstrates the promotion of subcritical growth of flaws at increasing heterogeneity of the ZrO_2 dispersion. With optimum homogeneity Fig. 4 predicts a strength of 800 to 900 MPa for the applied forming technology of bars.

According to Fig. 4, B-route technology seems to be favoured in comparison with Route A. This is, however, only true if the really best premises for high

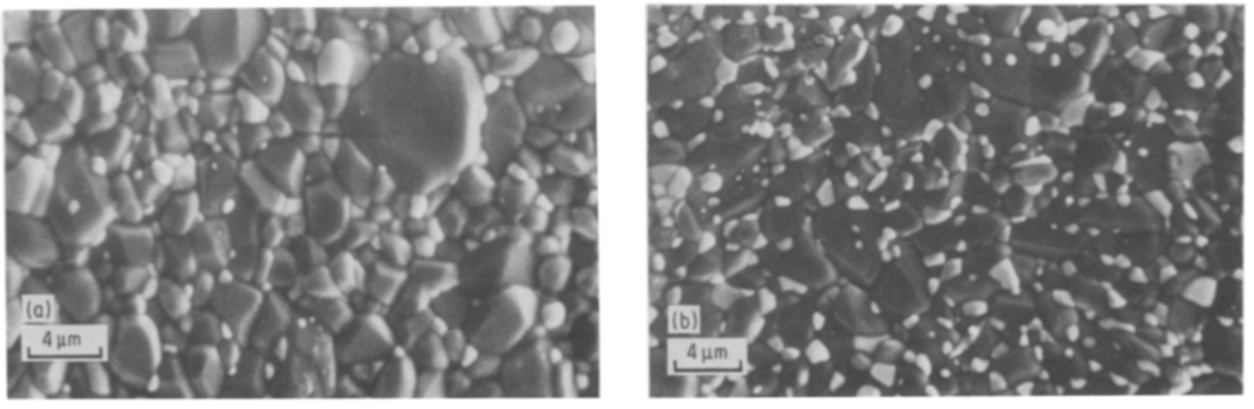

Figure 2 Distribution of ZrO_2 particles (bright) on as-sintered surfaces of A-route Al_2O_3 + 11.5 vol % ZrO_2. The ZrO_2 powder added had an average agglomerate size of (a) 1.1 µm, and (b) 0.65 µm. Sintering temperature 1625° C. Scanning electron micrograph.

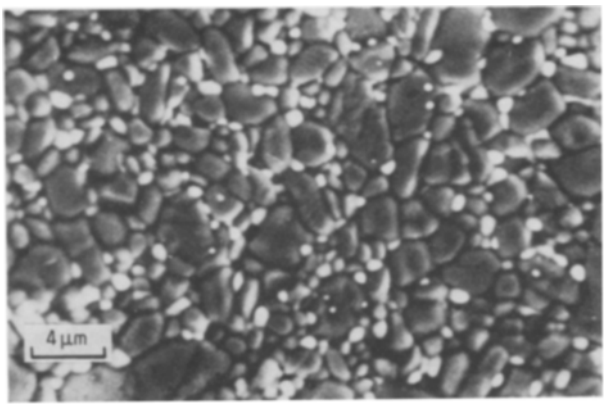

Figure 3 SEM micrograph of a polished and thermally etched (1450° C for 2 h in air) surface of B-route Al_2O_3 + 11.5 vol % ZrO_2. Sintering temperature 1560° C.

homogeneity (adding ZrO_2 as oxychloride solution) are combined with the most intense homogenization and appropriate granulation (Table II). Under such circumstances, maximum K_{Ic} values are realized with lower tetragonal contents (X_t = 0.35 at K_{Ic} = 11.8 MPa $m^{1/2}$), whereas high strength requires higher X_t values measurable on the as-sintered surface (X_t = 0.52 at σ_f = 629 MPa). From Table I the "true" K_{Ic} will be 7 to 9 MPa $m^{1/2}$ for structures giving 9 to 12 MPa $m^{1/2}$ in Table II.

3. Discussion

The excellent correspondence between K_{Ic} and ϱ^f_{abs} in Fig. 1 clearly demonstrates that microcrack toughening is the dominant mechanism in ZTA with X_t = 0.30 to 0.55. Note that only those microcracks are effective in energy dissipation which are generated during the macroscopic fracture process. Comparing the results at 0 and 7.5 vol % ZrO_2 it is evident that fewer microcracks in ZTA result in a higher fracture toughness than in Al_2O_3. This higher efficiency of the dissipating process in ZTA is associated with higher residual stresses due to the martensitic ZrO_2 transformation, and is theoretically well understood [2].

A further contribution to the measured high K_{Ic} may have originated from the observed independent microcracking around ZrO_2 particles and within zirconia-free subregions of the Al_2O_3 matrix (from high-voltage TEM [17]). As previously suggested [18], such a synergetic combination of mechanisms under special circumstances can give rise to an increase in K_{Ic} which is stronger than expected from the linear addition of energies.

Fig. 4 further substantiates the assumption that the known effect of heterogeneously distributed ZrO_2 particles on strength is due to the associated action of residual tension in the Al_2O_3 matrix. These residual stresses promote subcritical crack growth and generate large flaws at instability. Presumably the reduction of local tension is also the reason for the often observed correspondence of high strength with high X_t.

The more homogeneous of the two data sets given in Fig. 4 for 0.65 and 1.1 µm ZrO_2, respectively, relate to hydrogen sintering, while the two other structures had been sintered in air. At present, however, we are not sure that this difference is a systematically occuring reproducible effect.

The newly introduced parameters of homogeneity permit the quantitative description of conditions where fracture toughnesses, which are approximately doubled with respect to Al_2O_3, can be utilized to generate high strength levels around 200% of those characteristic for Al_2O_3. We suppose, therefore, that in this way further progress may lead to strengths of 800 to 1000 MPa even for pressureless sintered unground parts, i.e. without the need of supplementary macroscopic surface stresses.

4. Conclusions

The demonstrated correlation between microcrack density and fracture toughness gives evidence that energy dissipation by microcracking during macroscopic fracture is the dominant toughening mechanism in Al_2O_3 + ZrO_2. This process is the more effective the higher are the residual stresses within the structure.

The quantitative analysis of dispersion homogeneity signifies that individual submicrometre ZrO_2 particles really have to be homogenized on a micrometre scale if high toughness values are to be accompanied by high strength. To this end, intense homogenization under conditions of best mixing of the

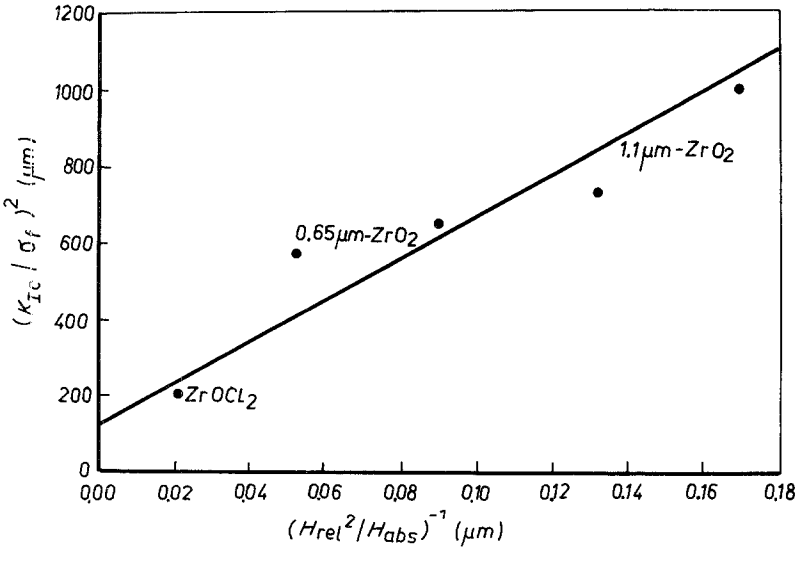

Figure 4 Influence of distribution homogeneity on flaw size at instability, characterized by the ratio $(K_{Ic}/\sigma_f)^2$ [16]. All analyses made on as-sintered surfaces. The structure fabricated with $ZrOCl_2$ is shown in Fig. 3; it is that with the highest strength in Table II and has X_t = 0.52.

TABLE II Influence of homogenization on averages of Young's modulus E, fracture strength σ_f and toughness K_{Ic} of B-route ZTA (all structures sintered in hydrogen)

Time of milling, type of drying/granulation, sintering temperature	E (GPa)	σ_f (MPa)	K_{Ic} (MPa $m^{1/2}$)
5 h, 0.63 mm sieve, 1580° C	321	329	–
10 h, 0.63 mm sieve, 1580° C	364	540	–
4 h, freeze-drying, 1560° C	350	500	7.7
8 h, freeze-drying, 1600° C	376	582	11.8
10 h, freeze-drying, 1560° C	375	629	9.1

different phases (use of solutions) must be complemented by drying and granulating technologies which guarantee the maintenance of that optimum homogeneity.

References

1. N. CLAUSSEN, *J. Amer. Ceram. Soc.* **59** (1976) 49.
2. W. POMPE and W. KREHER, in "Advances in Ceramics", Vol. 12 (Proceedings of 2nd International Conference on the Science and Technology of Zirconia), edited by N. Claussen, M. Rühle and A. H. Heuer (American Ceramic Society, Columbus, Ohio, 1983) p. 283.
3. N. CLAUSSEN, R. L. COX and J. S. WALLACE, *J. Amer. Ceram. Soc.* **65** (1982) C190.
4. A. H. HEUER, N. CLAUSSEN, W. M. KRIVEN and M. RÜHLE, *ibid.* **65** (1982) 642.
5. N. CLAUSSEN, *Z. Werkstofftechnik* **13** (1982) 138.
6. *Idem, ibid.* **13** (1982) 185.
7. M. V. SWAIN and N. CLAUSSEN, *J. Amer. Ceram. Soc.* **66** (1983) C27.
8. G. R. ANSTIS, P. CHANTIKUL, B. R. LAWN and D. B. MARSHALL, *ibid.* **64** (1981) 533.
9. *Idem, ibid.* **64** (1981) 539.
10. A. G. EVANS, *Mater. Sci. Engng.* **71** (1985) 3.
11. A. KRELL and D. SCHULZE, *Phys. Status Solidi (a)* **55** (1979) 537.
12. A. KRELL and D. SCHULZE, *Silikattechnik* **36** (1985) 294.
13. A. KRELL, *Phys. Status Solidi (a)* **63** (1981) 183.
14. A. KRELL and W. KREHER, *J. Mater. Sci.* **18** (1983) 2311.
15. B. BUDIANSKY and R. J. O'CONNELL, *Int. J. Sol. Struct.* **12** (1976) 81.
16. T. WEISS, submitted to *Pract. Metallography.*
17. J. WOLTERSDORF and E. PIPPEL, private communication.
18. W. POMPE, H.-A. BAHR and W. KREHER, *Neue Hütte* **30** (1985) 425.

Received 23 October 1986
and accepted 22 January 1987